Quantum Signatures in Laser-Driven Relativistic Multiple Scattering

Guido R. Mocken* and Christoph H. Keitel†

Theoretische Quantendynamik, Physikalisches Institut, Universität Freiburg, Hermann-Herder-Straße 3, D-79104 Freiburg, Germany

(Received 24 March 2003; published 24 October 2003)

The dynamics of an electronic Dirac wave packet evolving under the influence of an ultraintense laser pulse and an ensemble of highly charged ions is investigated numerically. Special emphasis is placed on the evolution of quantum signatures from single to multiple scattering events. We quantify the occurrence of quantum relativistic interference fringes in various situations and stress their significance in multiple-particle systems, even in the relativistic range of laser-matter interaction.

DOI: 10.1103/PhysRevLett.91.173202 PACS numbers: 34.80.Qb

The interplay of the strongest forces in atomic physics via ultraintense laser pulses and highly charged ions is governed rather well by quantum relativistic Dirac dynamics [1–3]. On one hand, for single particles, quantum effects such as tunneling, spin effects, and quantum interferences were shown to be rather crucial even in the relativistic regime [4,5]. On the other hand, for many particle systems, laser-induced plasma physics was shown to be remarkably well described by classical relativistic dynamics [6,7]. With the intermediate regime from few particle to cluster physics attracting increasing interest [8], the question arises for the role of quantum effects in laser-induced relativistic multiple-particle dynamics.

In this Letter, we investigate the quantum relativistic dynamics of laser-driven multiple scatterings of an electron being represented by a Volkov wave packet at an ensemble of highly charged ions. With a numerical accuracy, which allows for transitions even to the Dirac sea with negative energies, we quantify the interference fringes at each scattering event and the mutual interplay among those events. Clear quantum behavior in the Dirac wave packet is identified in the highly relativistic regime after multiple scattering.

The system of interest consists of an electron which is driven by an intense laser pulse with time t and space $\vec{r}$ dependent vector potential $\vec{A}(t, \vec{r})$ and scattered multiply at an ensemble of ions with scalar potential $A_0(\vec{r})$. The electronic wave packet dynamics in such an environment is characterized by the Dirac spinor $\psi(t, \vec{r})$ and is governed by the Dirac equation reading in atomic units as throughout the article:

$$i\hbar \frac{\partial \psi}{\partial t} = \left[\frac{\hbar c}{i} \alpha^j \frac{\partial}{\partial r^j} + \beta mc^2 + q(A_0 - \alpha^j A_j) \right] \psi, \quad (1)$$

with electron charge $q = -1$ a.u., electron mass $m = 1$ a.u. and α^j ($j \in \{1, 2, 3\}$), and β being the Dirac matrices [9]. The three components of $\vec{r}$ and $\vec{A}$ are r^j and A^j, respectively, and $c = 137.036$ a.u. the speed of light.

Our numerical analysis takes advantage of splitting the linear Dirac Hamiltonian into a position-dependent and a derivative-dependent part. We then make use of the so-called "split-operator" technique [10], in which we propagate the wave packet successively by the position- and derivative-dependent parts and employ fast-Fourier transformations, such that all operations are plain multiplications. With time step Δt, the numerical error introduced this way is of the order of Δt^3 [10]. For $\Delta t \approx 2 \times 10^{-5}$ a.u. $< \hbar/(2mc^2)$, transitions between positive- and negative-energy states are resolved, and this way we obtained convergence of our split-step propagation of ψ even at large $t \gtrsim 10$ a.u. Further, the spacing of our two-dimensional grid in position space needs to be suitable to resolve the maximal momenta employed. In spite of large relativistic velocities, this is not problematic, because it is the canonical rather than the kinetic momentum that has to be represented on the grid, with $\vec{p}_{\text{can}} - \frac{q}{c}\vec{A} = \vec{p}_{\text{kin}}$. In the case of a high velocity of the particle being exclusively due to an intense laser field, $\vec{p}_{\text{can}}$ is even zero in polarization direction $\vec{e}_2$. It is nonzero in propagation direction $\vec{e}_1$, but its magnitude is small even for intense fields. Once scatterings with nuclei have occurred, however, high canonical momenta appear, which, for the parameters used here, can be represented successfully on a grid with a spacing $\Delta x_i = 0.118$ a.u., corresponding to a maximum momentum of 26.6 a.u. The so-called fermion doubling problem, which occurs at momenta close to the highest grid momenta, is consequently also avoided [11].

For the sake of reducing computing power, we introduced two advantageous techniques. First, in position space, the calculation is restricted to the area centered around the rapidly moving wave packet, involving a "moving-grid" approach. Second, the grid size, too, is dynamically adapted in time: While a freely evolving wave packet spreads with time, a multiply scattered one does considerably more. As our simulation has to cover a substantial part of the whole laser pulse, including times where the packet is still quite small, it is possible to save considerable CPU time, noting that the time consuming two-dimensional fast-Fourier transformations scale as $O(N^2 \log N)$, where $N \times N$ equals the grid size. This "growing-grid" approach is also our pragmatic solution

to the well-known boundary problem [3,12] in Dirac calculations, at least to the point where damping functions and absorbing boundaries become unavoidable. The maximally introduced relative loss of normalization of the wave function, arising solely this way, is limited by 2.5% in our simulations to follow. Finally, the whole code is written to take advantage of multiple CPUs.

In a series of contour plots, we present the time evolution of an initially Gaussian shaped wave packet under the influence of a strong laser pulse, which is subsequently scattered at several highly charged ions. We use a four cycle laser pulse with amplitude $E_0 = 50$ a.u. ($I = 8.75 \times 10^{19}$ W/cm^2) and frequency $\omega = 1$ a.u., which features a 1.5 cycle $\sin^2$ turn-on and turn-off, and one cycle of constant intensity in between. As amplitude and frequency suggest, we are clearly in the fully relativistic regime. The ions are modeled by static softcore potentials $Ze^2/\sqrt{[(\vec{r} - \vec{r}_{\mathrm{Ion}})^2 + a]}$, with a "Coulomb-like" small softcore parameter $a = 0.01$ being just large enough to avoid numerical instabilities at the ions' origins $\vec{r}_{\mathrm{Ion}}$. We chose their charge as a high multiple ($Z = 50$) of the elementary charge e to acquire comparable field strengths for laser and ions (at 1 a.u. distance from the ionic center).

In Fig. 1, the top left graph illustrates an overview of the successive quantum relativistic scattering scenario of an electron wave packet at two highly charged ions. The initial Gaussian wave packet (full width 2 a.u. in momentum space at $1/e$th of the maximal height, and solely with positive energy and spin up with respect to $\vec{e}_1 \times \vec{e}_2$) is centered around the origin and its evolution is depicted by various snap shots along its center of mass motion (solid line) in the laser pulse. At first, after a short motion in the negative polarization and positive propagation directions during the first half cycle of the turn-on phase, the particle is visibly accelerated in the polarization direction, reaching the first upper turning point after the first

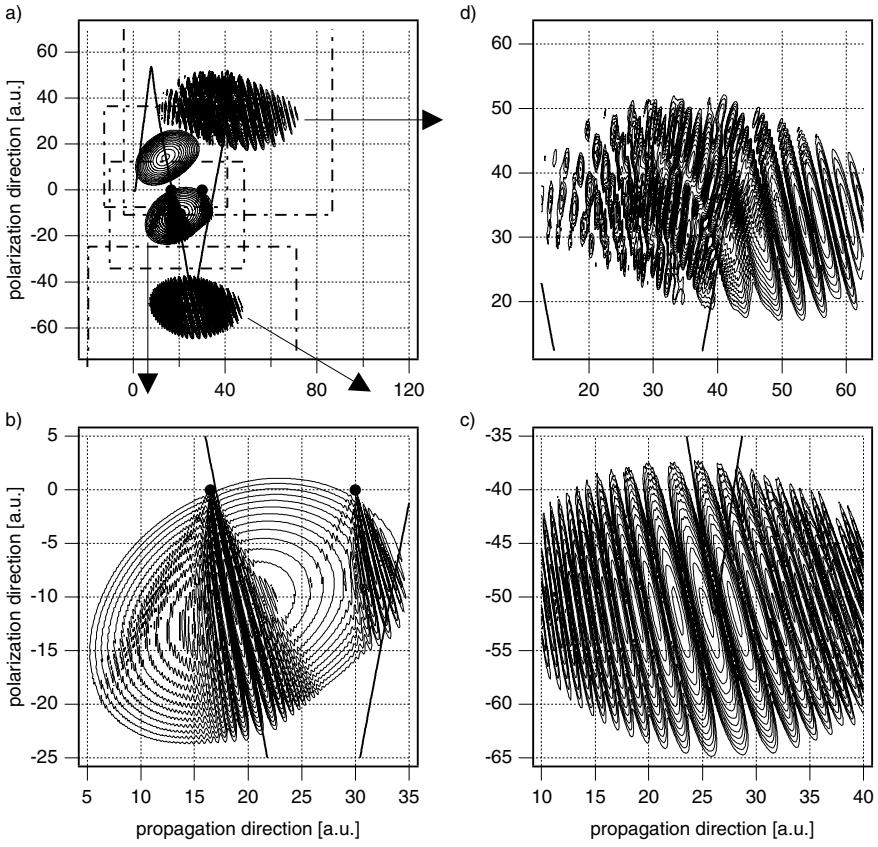

FIG. 1. (a) Overview: Contour plots at $t = 7.645$, 8.195, 9.495, and 12.095 a.u. corresponding to times before the first scattering, shortly after it, at the lower point of return, and after the second scattering, close to the upper point of return. The four dashed rectangles (some only partly visible) mark the dynamical grid boundaries for each of these situations. The thick dots indicate the positions of two Sn^{50+} ions, which are located right on the horizontal axis at positions 16.5 and 30.0 a.u. The solid line depicts the trajectory of the expectation value of the particle's spatial coordinate. We omit any enlarged view of the initially Gaussian packet at $t = 7.645$ a.u., but provide them for the other three cases as follows: (b) enlarged view at $t = 8.195$ a.u. showing single scattering fringes shortly after the scattering event; (c) enlarged view at $t = 9.495$ a.u. that depicts the same single scattering fringes somewhat later in order to illustrate the growth of the distance between any two fringes [compare with (b)]; (d) enlarged view at $t = 12.095$ a.u. which displays interference from two separate scattering events with crossed fringes on the left side and on the right side the unperturbed structure from the first scattering event. In all cases, 20 contour lines are shown for $|\psi|^2$ with constant steps within $-1.15 \geq \log|\psi|^2 \geq -4$.

whole cycle is completed. Further on, continuing with a clear Lorentz-force induced drift in the laser propagation direction, the electron wave packet is accelerated in the negative polarization direction to face its first encounter with an ionic core potential. The motion that we observe during the first unperturbed $1\frac{1}{4}$ cycles could be modeled rather accurately and easily with a classical Monte Carlo ensemble and is completely in agreement with known free (without nucleus) quantum wave packet results in [13]. This includes the Lorentz contraction of the wave packet along the direction of present velocity and its apparent rotation, i.e., precisely shearing, because of the phase differences sensed by spatially separated parts of the wave packet.

At the first encounter of the electron wave packet with the nucleus at position (16.5,0), the laser electric field is rather small at this particular phase. Therefore relativistic Coulomb scattering dominates, involving the interference of the incoming wave with the scattered wave. The corresponding fringe structure, which features a distinct maximum in the forward direction followed by a series of side maxima, can be viewed in detail in Fig. 1(b). Further fringes from a scattering at the second ion at (30,0) are also visible. The small oscillations present numerical noise: As opposed to the much higher quantum interference structures in the logarithmic plot, they vary with increasing spatial grid sizes. The probability for the negative-energy states, which are almost purely in the continuum, is clearly enhanced during the scattering, remains though still well below 5% then and afterwards. Relative deviations due to the spin degree of freedom increase up to ca. 10^{-5} at the scattering event for our parameters. This can be estimated by relating the spin-orbit energies to the total system energy and by redoing the calculations in Fig. 1 with spin-down polarization initially. With increasing time, the wave packet evolves in the negative polarization direction towards the second lower turning point, which is reached after 1.5 cycles. The separations among the fringes have grown substantially which themselves turn continuously more parallel, with an orientation reflecting the direction of motion at the time when the scattering occurred [Fig. 1(c)].

Finally, the wave packet, which at this stage is split into various fractions, continues in the positive polarization direction. The fringes maintain their orientation when the second scattering at the second ion occurs, and are therefore joined by a set of newly created fringes with a different orientation. When two cycles are completed, the electron has reached its second upper turning point. Figure 1(d) is a snapshot taken a little while before that, and one can clearly see the pattern that is generated by two sets of differently oriented interference fringes. From then on, without further scatterings, the whole structure essentially remains, apart from further changes imposed by the laser field such as spreading and shearing with an essentially classical center-of-mass motion.

In Fig. 2, we show in a similar way the effect on the same initially Gaussian wave packet after it has passed a collection of seven ions two times. A classical estimation confirms that such a collection of heavy highly charged ions moves less than 0.04 a.u. due to Coulomb repulsion and the laser field during maximally employed interaction time of $\Delta t \approx 12$ a.u. and may thus be assumed as resting. We note that the clear interference structures in single and double scattering are now less apparent though still visible when one moves to complex structures.

A simple analytical model is finally introduced to qualitatively confirm our numerical result. Adopting the existing textbook [14] theory for three-dimensional Dirac scattering of an electron ψ at the time-independent potential of an ion at $\vec{r}_{\mathrm{Ion}} = \vec{0}$, we obtain

$$\psi(\vec{r}) = \phi(\vec{r}) - \int d^3r' G_0(\vec{r}, \vec{r}', E) V(\vec{r}') \psi(\vec{r}'), \qquad (2)$$

with unperturbed Dirac wave $\phi(\vec{r}) = w^{\rho}(\vec{p}) e^{(i/\hbar)\vec{p}\cdot\vec{r}}$ ($\rho \in \{1, 2\}$ depending on spin), corresponding eigenvalue E, and $w^{\rho}(\vec{p})$ being the free-electron spinor amplitude [9]. On the right-hand side of Eq. (2), we replace ψ by ϕ (first

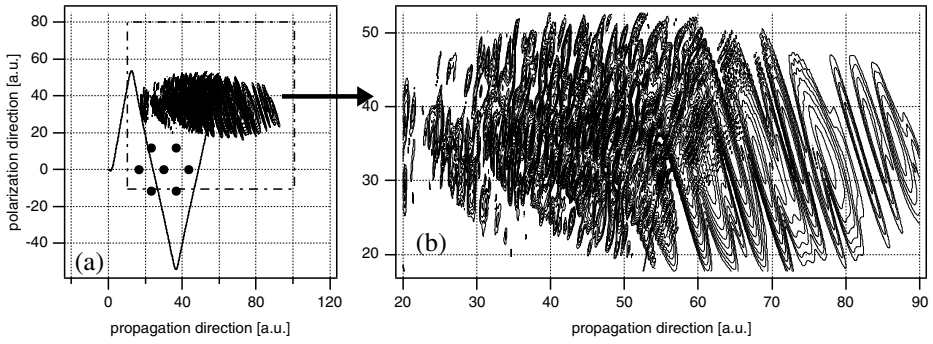

FIG. 2. (a) Overview: Contour plots at time $t = 12.270$ a.u. after two scatterings at an ensemble of six Sn^{50+} ions (thick dots) centered symmetrically around a further one at position (0,30) a.u. The dashed rectangle marks the grid boundary and the solid line depicts the trajectory of the expectation value of the electron's spatial coordinate. (b) This enlarged view of the wave packet in (a) illustrates how the two scattering events at seven ions modify the regularity in the interference pattern. In both graphs, 20 contour lines are shown for $|\psi|^2$ with constant steps within $-1.15 \geq \log|\psi|^2 \geq -4$.

Born approximation) and insert the relativistic free-particle Green's function at energy E [14]:

$$G_0(\vec{r},\vec{r}',E)=\frac{1}{\hbar c}[c\vec{\alpha}\cdot\underline{\vec{p}}+\beta mc^2+E]\frac{e^{(i/\hbar)pR}}{4\pi R}, \quad (3)$$

where $R=|\vec{r}-\vec{r}'|$, $p=\sqrt{(E^2/c^2)-(mc)^2}$, $\underline{\vec{p}}=-i\hbar\vec{\nabla}$, $\vec{p}$ is the initial momentum, $\vec{p}'=(p\vec{r})/r$ is the final momentum, and $p=\hbar k=|\vec{p}|=|\vec{p}'|$ its magnitude. For the case of interest $r\gg r'$, neglecting contributions of order $1/r^2$ and higher, and assuming a short-range potential, one finally obtains the outgoing electronic wave function:

$$\psi(\vec{r})=w^{\rho}(\vec{p})e^{(i/\hbar)\vec{p}\cdot\vec{r}} - \frac{1}{4\pi(\hbar c)^2}[\vec{\alpha}\cdot\vec{p}'+\beta mc^2+E(\vec{p}'^2)]\frac{e^{(i/\hbar)p|\vec{r}|}}{|\vec{r}|} \times\int d^3r'\,V(\vec{r}')w^{\rho}(\vec{p})e^{(i/\hbar)(\vec{p}-\vec{p}')\cdot\vec{r}'}. \quad (4)$$

We are interested in the maxima of $|\psi|^2=\psi^{\dagger}\psi$, or more exactly in the angles ϑ_n that point towards the scattering fringes. Using $V(\vec{r}')=-V_0\delta(\vec{r}')$ [15] with $V_0>0$ as the simplest potential, we finally obtain, up to an additive function $f(r)$ and a constant prefactor, the ϑ-dependent part of $|\psi|^2$ as

$$|\psi|^2\propto[(\gamma^2-1)\cos\vartheta+1+\gamma^2]\cos(kr-kr\cos\vartheta)+f(r). \quad (5)$$

In the nonrelativistic case $\gamma=E/(mc^2)\approx 1$, the maxima of the above expression can be simplified further to read

$$\vartheta_n=\pm\arccos\left(1-\frac{n\pi}{kr}\right), \qquad n\in\mathbb{N}. \quad (6)$$

Then to adapt the dynamics in the laser fields, one may choose for a fixed initial momentum $\hbar k$ a distance r where, in the *absence* of a laser field, the scattering fringes would be observed and calculate the corresponding angles ϑ_n. Then with the laser field and using a classical formula [16] and now neglecting the ionic potentials, one may propagate over a period $t=(mr)/(\hbar k)$ a suitably chosen ensemble of classical particles that initially starts at the position of the scattering center with initial momenta of magnitude $\hbar k$ in the direction of the scattering angles ϑ_n. This simple model qualitatively confirms our numerical results while it fails to predict the final positions and separations of the fringes by better than a factor of 2. In addition to the stressed approximations in the analytical approach, the mimicking of the quantum wave packet in the transition regime from scattering to free dynamics in the laser field is too delicate to compete seriously in accuracy with the *fully* quantum relativistic approach.

In conclusion, the investigated multiple-particle system shows that there is an intermediate regime in the number of involved particles with clear quantum relativistic effects. While restrictions for multiple-particle classical relativistic calculations are pointed out, our results are of likely significance also for future experiments on laser-driven relativistic few-body and cluster dynamics.

Financial support by the German Science Foundation (SFB276) and helpful discussions with K. Z. Hatsagortsyan on spin-related issues are gratefully acknowledged.

*Electronic address: mocken@physik.uni-freiburg.de
†Electronic address: keitel@uni-freiburg.de
URL: http://tqd1.physik.uni-freiburg.de/~chk/a11/index_de.html

[1] P. H. Mokler and T. Stöhlker, Adv. At. Mol. Opt. Phys. **37**, 297 (1996); *TESLA Technical Design Report*, edited by G. Materlik and T. Tschentscher (DESY, Hamburg, 2001).
[2] C. J. Joachain *et al.*, Adv. At. Mol. Opt. Phys. **42**, 225 (2000); C. H. Keitel, Contemp. Phys. **42**, 353 (2001).
[3] A. Maquet and R. Grobe, J. Mod. Opt. **49**, 2001 (2002).
[4] U. W. Rathe *et al.*, J. Phys. B **30**, L531 (1997); J. W. Braun *et al.*, Phys. Rev. A **59**, 604 (1999).
[5] F. V. Bunkin and M. V. Fedorov, Zh. Eksp. Teor. Fiz. **49**, 1215 (1965) [Sov. Phys. JETP **22**, 844 (1966)]; C. Szymanowski *et al.*, Phys. Rev. A **56**, 3846 (1997); P. Panek *et al.*, Phys. Rev. A **65**, 033408 (2002).
[6] P. Gibbon and E. Förster, Plasma Phys. Controlled Fusion **38**, 769 (1996); G. Pretzler *et al.*, Phys. Rev. E **58**, 1165 (1998); K. W. D. Ledingham *et al.*, Phys. Rev. Lett. **84**, 1459 (2000); H. Schwoerer *et al.*, Phys. Rev. Lett. **86**, 2317 (2001); M. Zepf *et al.*, Phys. Rev. Lett. **90**, 064801 (2003).
[7] S. Hain and P. Mulser, Phys. Rev. Lett. **86**, 1015 (2001); Z.-M. Sheng *et al.*, Phys. Rev. Lett. **88**, 055004 (2002).
[8] S. X. Hu and Z. Z. Xu, Appl. Phys. Lett. **71**, 2605 (1997); T. Ditmire *et al.*, Nature (London) **398**, 489 (1999); G. Grillon *et al.*, Phys. Rev. Lett. **89**, 065005 (2002); M. Schulz *et al.*, Nature (London) **422**, 48 (2003).
[9] J. Bjorken and S. D. Drell, *Relativistic Quantum Mechanics* (McGraw-Hill, New York, 1964).
[10] J. Fleck *et al.*, Appl. Phys. **10**, 129 (1976); M. R. Hermann and J. A. Fleck, Phys. Rev. A **38**, 6000 (1988).
[11] C. Müller, N. Grün, and W. Scheid, Phys. Lett. A **242**, 245 (1998); L. Susskind, Phys. Rev. D **16**, 3031 (1977).
[12] V. Alonso *et al.*, Eur. J. Phys. **18**, 315 (1997).
[13] J. S. Román *et al.*, Phys. Rev. A **64**, 063402 (2001); J. Phys. B **33**, 1869 (2000).
[14] P. Strange, *Relativistic Quantum Mechanics* (Cambridge University Press, Cambridge, England, 1998), p. 410.
[15] F. H. M. Faisal and T. Radożycki, Phys. Rev. A **47**, 4464 (1993); **48**, 554 (1993); D. B. Milošević, S. X. Hu, and W. Becker, Phys. Rev. A **63**, 011403(R) (2001).
[16] Y. I. Salamin and F. H. M. Faisal, Phys. Rev. A **54**, 4383 (1996).